HHS Public Access

Author manuscript

Acta Biomater. Author manuscript; available in PMC 2021 May 01.

Published in final edited form as:

Acta Biomater. 2020 May ; 108: 142–152. doi:10.1016/j.actbio.2020.03.014.

Tunable Fibrin-Alginate Interpenetrating Network Hydrogels to Support Cell Spreading and Network Formation

Charlotte E. Vorwald[a], **Tomas Gonzalez-Fernandez**[a], **Shreeya Joshee**[a], **Pawel Sikorski**[b], **J. Kent Leach**[a,c,*]

[a]Department of Biomedical Engineering, University of California, Davis, Davis, CA, 95616

[b]Department of Physics, Norwegian University of Science and Technology (NTNU), Trondheim, Norway

[c]Department of Orthopaedic Surgery, UC Davis Health, Sacramento, CA 95817

Abstract

Hydrogels are effective platforms for use as artificial extracellular matrices, cell carriers, and to present bioactive cues. Two common natural polymers, fibrin and alginate, are broadly used to form hydrogels and have numerous advantages over synthetic materials. Fibrin is a provisional matrix containing native adhesion motifs for cell engagement, yet the interplay between mechanical properties, degradation, and gelation rate is difficult to decouple. Conversely, alginate is highly tunable yet bioinert and requires modification to present necessary adhesion ligands. To address these challenges, we developed a fibrin-alginate interpenetrating network (IPN) hydrogel to combine the desirable adhesion and stimulatory characteristics of fibrin with the tunable mechanical properties of alginate. We tested its efficacy by examining capillary network formation with entrapped co-cultures of mesenchymal stromal cells (MSCs) and endothelial cells (ECs). We manipulated thrombin concentration and alginate crosslinking density independently to modulate the fibrin structure, mesh size, degradation, and biomechanical properties of these constructs. In IPNs of lower stiffness, we observed a significant increase in total cell area ($1.7\times10^5 \pm 7.9\times10^4$ μm^2) and decrease in circularity (0.56 ± 0.03) compared to cells encapsulated in stiffer IPNs ($4.0\times10^4 \pm 1.5\times10^4$ μm^2 and 0.77 ± 0.09, respectively). Fibrinogen content did not influence capillary network formation. However, higher fibrinogen content led to greater retention of these networks confirmed *via* increased spreading and presence of F-actin at 7 days. This is an elegant platform to decouple cell adhesion and hydrogel bulk stiffness that will be broadly useful for cell instruction and delivery.

*Address for correspondence: J. Kent Leach, Ph.D., Department of Biomedical Engineering, University of California, Davis, 451 Health Sciences Drive, Davis, CA 95616, jkleach@ucdavis.edu.

CONFLICT OF INTEREST

The authors have no conflict of interest.

DATA AVAILABILITY STATEMENT

Data supporting the findings of this manuscript are available from the corresponding author upon reasonable request.

Graphical Abstract

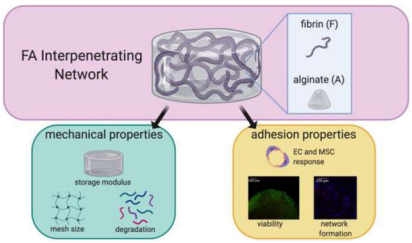

Keywords

Interpenetrating network; endothelial cell; mesenchymal stromal cell; fibrin; alginate

INTRODUCTION

Hydrogels are widely utilized in the pharmaceutical, biotechnology, and biomedical industry due to their high water content that mimics native tissues, biocompatibility, and cell-friendly nature. Hydrogels derived from natural polymers are particularly promising, as they present native adhesion ligands to support cell interaction with the material. Fibrin is broadly used since it is abundant during the innate, wound healing process and can stimulate reparative cellular activities [1]. Fibrin exhibits both vasculogenic and anti-inflammatory potential for wound healing and tissue repair [2, 3]. Although this material enables cell infiltration and remodeling [4], it is relatively compliant and difficult to handle when implanted. Current formulations used in the clinic involve fibrin clotting components at supraphysiological doses, resulting in fast gelation times that add deleterious stress on encapsulated cells.

Alginate is another widely used natural polymer to formulate hydrogels for biological applications because it possesses tunable mechanical properties, induces little inflammation, and is amenable to a variety of crosslinking methods [5]. As alginate is a bioinert polymer, it requires covalent modification with adhesive motifs to enable cell adhesion. This has been achieved using a variety of ECM components, with adhesive peptides such as Arginine-Glycine-Aspartic Acid (RGD) being the most common [6]. Peptides that are covalently bound to the polymer backbone promote adhesion but fail to mimic the complex nature of the ECM, while chemical modification of polymers with full sequence proteins is inefficient and may have interactions with other components that impair crosslinking.

Interpenetrating networks (IPNs) represent a promising solution to these hurdles and are created by a combination of two or more distinct hydrogel systems. In IPNs, networks are interlaced with each other but not chemically bonded [7]. IPNs possess increased functionality compared to individual polymers and have been used in numerous applications including drug delivery, wound healing, and tissue engineering [8]. Each hydrogel system is crosslinked through distinct mechanisms, either simultaneously or in parallel. Among polymers used in IPNs, alginate is commonly studied due to its tunable, robust mechanical properties. IPNs have been formed by combining collagen-alginate [9, 10], basement membrane-alginate [11], fibrin-alginate [12], and others. Collagen and basement membrane

are matricellular proteins present in mature tissues. Thus, fibrin-alginate IPNs would seem particularly promising due to the provisional nature of the fibrin, coupled with the tunability of the alginate. However, there is limited knowledge regarding the interplay between crosslinking mechanism, subsequent changes in biophysical properties of fibrin-alginate IPNs and resulting cell response.

Herein, we describe the fabrication and characterization of a fibrin-alginate IPN (FA IPN) to balance the compliance of fibrin with the mechanical stability and tunability of alginate. We hypothesized that FA IPNs would exhibit tunable mechanical and adhesive properties while supporting cell co-culture for use in vascularized tissue constructs. We report a unique method to create these constructs that retains fibrin structure within a dense alginate network. Fibrin-alginate IPNs formed using extrusion techniques yielded fibrin fiber diameters that were influenced by thrombin concentration [12], yet this strategy does not allow one to decouple the gelation rates of individual polymers in the IPN. Herein, we utilized light reflection microscopy, a non-invasive, label-free imaging modality, to confirm changes in fibrin structure and evaluate IPN structural properties. We used clinically relevant cell sources to test the efficacy of these IPNs, namely endothelial cells (ECs) and mesenchymal stromal cells (MSCs), which synergistically promote wound healing through capillary network formation [13]. EC-MSC response was dependent on alginate crosslinking density and fibrinogen content. These studies confirm, for the first time, the complete formation of fibrin structure in alginate to maximize the utility of the IPN. This work provides insight into the interplay of mechanical properties and cell spreading on capillary formation and retention and establishes FA IPN as a promising biomaterial for biomedical applications.

MATERIALS AND METHODS

IPN synthesis

UltraPure MVG sodium alginate (molecular weight >200,000 g/mol, Pronova, Lysaker, Norway) was oxidized to a degree of oxidation of 1% with sodium periodate (MilliporeSigma, St. Louis, MO) as previously described [14] and dissolved in PBS at 3% w/v. Fibrinogen (MilliporeSigma) was mixed with alginate solution at 30 mg/mL and allowed to dissolve at 37°C in PBS overnight. This solution remained sterile and stored at 4°C until use for subsequent experiments.

3.5 kDa MWCO dialysis membranes (Spectrum Labs, Rancho Dominguez, CA) were hydrated in sterile ultrapure water for at least 10 min. We prepared solutions of calcium chloride ($CaCl_2$, MilliporeSigma) in water at 10 mM or 40 mM. To obtain a 2% w/v alginate and 20 mg/mL fibrinogen IPN, 66 μL of fibrinogen-alginate solution was mixed with 33 μL of thrombin solution with a concentration range of 0–75 U/mL, and 80 μL was immediately pipetted into 8 mm circular, silicon molds. Fibrin networks were allowed to form for 45 min at 37°C. A hydrated dialysis membrane was then placed gently on top of molds, and $CaCl_2$ solution was pipetted on top until fully covered. Alginate was allowed to crosslink for 30 min at 37°C. Resulting constructs were gently transferred from molds to non-coated 8-well chamber slides (ibidi, GmbH, Planegg, Germany).

Fibrin characterization *via* light reflection and confocal microscopy

66 μL of fibrinogen-alginate solution was mixed with 33 μL of thrombin (75 U/mL, 7.5 U/mL, and 0.75 U/mL) and pipetted directly into non-coated 8-chamber wells (ibidi) for a resulting fibrinogen and thrombin concentration of 20 mg/mL and 25 U/mL, 2.5 U/mL, and 0.25 U/mL, respectively. Fibrin was allowed to form for 45 min at 37°C. Reflection confocal microscopy was performed using the Leica TCS SP8 (Leica, Wetzlar, Germany) using a 600 nm laser line and detector (586–624 nm) at 40X magnification to observe fibrin structure within FA IPN hydrogels.

Gelation kinetics measurements of fibrin in alginate

66 μL of fibrinogen-alginate solution was mixed with 33 μL of thrombin for a resulting fibrinogen and thrombin concentration of 20 mg/mL and 25 U/mL, 2.5 U/mL, and 0.25 U/mL, respectively. 50 μL was pipetted directly into each well of a flat, clear 96-well plate. Optical density was measured at 350 nm and 550 nm in triplicate at 4 min intervals for 45 min at 37°C. Similar trends from 350 nm and 550 nm readings ensured that results were due to light scattering and not due to absorption [15]. Fibrin with respective thrombin concentrations served as positive controls. PBS, FA without thrombin, and fibrinogen without thrombin served as negative controls.

Characterization of IPN physical properties

Viscoelastic properties of acellular IPNs were measured on a Discovery HR-2 hybrid stress-controlled rheometer (Thermal Analysis Instruments, New Castle, DE) equipped with an 8 mm parallel plate geometry. Gels were tested at a strain of 0.5% and frequency sweep from 0.1 to 10 rad/s. The storage modulus was reported at 1.58 rad/s.

Mesh size, r_{mesh}, was calculated from data based on rheological measurements [16] and approximated by the following equation:

$$r_{mesh}\left(\frac{6 * RT}{\pi N_{av} G}\right)^{1/3}$$

where R is the gas constant, T is the absolute temperature, N_{av} is Avogadro's number, and G is the storage modulus. Initial storage modulus of crosslinked gels was measured, and gels were subsequently weighed to obtain wet weight. Constructs were then frozen at −80°C overnight, lyophilized for 1 day, and weighed again to obtain dry weight.

Cell culture

Human cord blood-derived endothelial colony forming cells (ECs) were kindly provided by Prof. Eduardo Silva (UC Davis) and expanded in EGM-2 supplemented media (PromoCell, Heidelberg, Germany) with gentamycin (50 μg/mL; Invitrogen, Carlsbad, CA) and amphotericin B (50 ng/mL; Invitrogen) under standard conditions (37°C, 5% CO_2, 21% O_2) until use at passage 5 [17]. Human bone marrow-derived MSCs (Lonza, Walkersville, MD) from a single donor (22 year-old male) were expanded without further characterization in growth medium (GM) consisting of minimum essential alpha medium (α-MEM; Invitrogen) supplemented with 10% fetal bovine serum (FBS; Atlanta Biologicals, Flowery Branch,

GA) and 1% penicillin/streptomycin (Gemini Bio-Products, Sacramento, CA). MSCs were cultured under standard conditions until use at passage 5. Media changes were performed every 2–3 days. For each experiment, aliquots were derived from the same batch of serum to ensure consistency.

EC-MSC encapsulation in FA IPN constructs

ECs and MSCs were suspended in fibrin-alginate solution at 1×10^6 cells/mL and 2×10^6 cells/mL, respectively, for a total concentration of 3×10^6 cells/mL [18, 19]. 66 μL of fibrin-alginate cell suspension was mixed with 33 μL of thrombin for a resulting fibrinogen and thrombin concentration of 20 mg/mL and 2.5 U/mL, respectively unless specified otherwise. 80 μL was pipetted directly into 8 mm silicon molds. Fibrin was allowed to form for 45 min at 37°C. Meanwhile, a hydrated dialysis membrane was placed gently on top of molds, and $CaCl_2$ solution was added on top until fully covered. Alginate was allowed to crosslink for 30 min at 37°C. Resulting FA IPN constructs were gently transferred from molds to non-coated 8-chamber slides (ibidi) and cultured in 250 μL 3:1 EGM-2: α-MEM under standard conditions. Media was refreshed every 48 hours.

Evaluation of cell spreading within IPNs using confocal microscopy

Before encapsulation, ECs were stained with CellTrace™ Violet (Invitrogen) and MSCs were stained with CellTrace™ Far Red Cell Proliferation Kit (Invitrogen). Co-culture of ECs and MSCs are denoted as “EC-MSC” within this manuscript. Confocal microscopy was performed using the Leica TCS SP8 on day 1, 3, and 7 of culture. Images were processed and analyzed in ImageJ (NIH, Bethesda, MD). Confocal images were converted to 500 × 500 pixel size, converted to binary, and circularity and area of cells with an area of at least 50 μm^2, well below the average size of ECs [20], were measured. Values are reported by cell population channel acquired for each material group. At day 7 of culture, gels were fixed with 4% paraformaldehyde at 4°C overnight, washed twice with PBS, and permeabilized with 0.05% Triton-X 100 for 5 min at room temperature. Gels were stained with Alexa Fluor 488 Phalloidin solution (Thermo Fisher, Waltham, MA; 1:40 in PBS) and incubated at room temperature for 1 hr. Gels were washed twice with PBS and subsequently imaged using confocal microscopy.

Evaluation of cell viability and metabolic activity

Cell viability was assessed by a LIVE/DEAD assay per the manufacturer’s protocol (Thermo Fisher). To measure metabolic activity, gels were transferred to 24-well plates and incubated in 500 μL 3:1 EGM-2:alpha MEM containing 10% v/v alamarBlue (Thermo Fisher) for 1 hr. Absorbance was read at 570 nm and 600 nm, and percent reduction was calculated as indicated by the manufacturer.

PCR

Gels were incubated in 10 U/mL alginate lyase (Sigma) and 50 U/mL nattokinase (NSK-SD, Japan Bio Science Laboratory Co., Osaka, Japan) in PBS containing 1 mM EDTA (Thermo Fisher) for 45–90 min at 37°C and pelleted *via* centrifugation as described [21]. Total RNA was collected and isolated in Trizol (Thermo Fisher), and 800 ng of total RNA was reverse

transcribed with the QuantiTect Reverse Transcription Kit (Qiagen, Germantown, MD). qPCR was performed using TaqMan1 Universal PCR Master Mix (Thermo Fisher). Primers and probes consisted of *VEGFA* (Hs00900055_m1). Amplification conditions were 50°C for 2 min, 95°C for 10 min, followed by 40 cycles at 95°C for 15 s and 60°C for 1 min. Quantitative PCR results were normalized to *RPL13* (Hs00744303_s1) transcript level to yield ΔCt. Values are represented as $2^{-\Delta Ct}$.

Histological analysis and immunofluorescent detection of CD31 and αSMA

Gels were fixed in 4% paraformaldehyde overnight at 4°C and washed in ultrapure water. Samples were dehydrated in a graded series of ethanol baths and paraffin-embedded overnight. Each gel was sectioned at 7 μm thickness using a Leica RM2235 Manual Rotary Microtome and affixed to microscope slides for subsequent staining. For CD31 and alpha smooth-muscle actin (αSMA) immunofluorescence (IF), slides were dehydrated and processed for antigen retrieval using chondroitinase ABC (Millipore Sigma). Primary antibodies against CD31 (1:20; ab28364, Abcam, Cambridge, MA) and SMA (1:50; ab7817, Abcam) were incubated overnight at 4°C [18]. Biotin-conjugated anti-rabbit (1:100; ab6720, Abcam) and anti-mouse (1:200; B7151, Sigma) secondary antibodies were added and incubated at room temperature for 1 hr. ExtrAvidin-FITC and -Cy3 (1:100; Sigma) were added to CD31 and SMA samples, respectively, and incubated for 1 hr at room temperature. DAPI (2 μg/mL; Thermo Fisher) was added and incubated at room temperature for 10 min and mounted with VECTASHIELD Antifade Mounting Medium (Vector Laboratories, Burlingame, CA). Images were acquired *via* fluorescence microscopy with the Nikon Eclipse TE2000U.

Statistical analysis

Data are presented as means ± standard deviation. Statistical significance was assessed by either one-way ANOVA, two-way ANOVA with Tukey's multiple comparisons test, or Student's t-test when appropriate. p-values <0.05 were considered statistically significant. Statistical analysis was performed using GraphPad Prism® 8 analysis software (GraphPad Software, La Jolla, CA). Different letters denote statistical significance between groups, while data sharing a letter are not statistically different from one another.

RESULTS

Fibrin structure and gelation of IPNs are dependent on thrombin concentration

The formation of uniform, well-formed fibrin fibers within the alginate solution before alginate crosslinking occurs was a key design criterion for successful IPN formulation, as this is representative of mature, fibrin fibers found in blood clots [22]. To determine the interplay of thrombin concentration and fibrin fiber morphology, we assessed fibrin structure within crosslinked alginate using confocal reflection microscopy. We observed a striking increase in fibrin thickness and reduced alignment as thrombin concentration increased (Fig. 3A). Fibrin control gels exhibited decreased mesh size with increasing thrombin concentrations. Fibrin structure for gels crosslinked with both 0.25 and 2.5 U/mL thrombin possessed a consistent mesh size throughout the gel. However, fibrin gels made with 25 U/mL thrombin possessed a dense, fine mesh with large, open pockets. We observed more

open mesh structure with thicker fibers in IPNs compared to fibrin controls of corresponding thrombin concentration. In IPNs, we also observed increased density of fibrin structures as thrombin concentration increased.

To explore the kinetics of gelation in IPNs, we measured gel turbidity and storage modulus during the gelation process of fibrin and alginate, respectively (Fig. 3B–C). Turbidity, measured by optical density (O.D.), increased as the fibrin fibers were formed [15] (Fig. 3B). We compared fibrin formation in fibrin controls and fibrinogen-alginate solutions. At 45 minutes, PBS and fibrinogen without thrombin showed minimal O.D. (0.03 ± 0.0 and 0.1 ± 0.0, respectively), as expected. IPNs without thrombin exhibited higher initial and resulting O.D. (0.4 ± 0.3) compared to both PBS and fibrin without thrombin. O.D. increased for fibrin gels as thrombin concentration increased. Fibrin with 0.25 U/mL thrombin showed a slow increase in O.D. over time, while fibrin gels made with 2.5 and 25 U/mL thrombin demonstrated a striking increase in overall O.D. values over 45 minutes. Similarly, O.D. increased in IPNs with increasing thrombin concentrations. However, IPN O.D. was highest with 0.25 U/mL thrombin (1.1 ± 0.1) compared to 2.5 U/mL (0.7 ± 0.3) and 25 U/mL thrombin (0.7 ± 0.5). The storage modulus of alginate increased as a function of crosslinking time (Fig. 3C). In alginate constructs crosslinked with 10 mM $CaCl_2$, we observed increase in storage modulus from 10 to 30 min gelation time, yet no statistical differences across all gelation times. For alginate constructs crosslinked with 40 mM $CaCl_2$, we observed a significant increase in storage modulus from 10 to 30 min gelation time (1187 ± 1309 and 3017 ± 731 Pa). No differences were observed between 30 and 60 min of gelation in either group, suggesting that alginate was fully crosslinked by calcium at 30 min.

To understand the contribution of fibrin structure on degradation kinetics of FA IPNs, fibrin and alginate were fully crosslinked with 2.5 U/mL thrombin and 10 mM $CaCl_2$, respectively, and we measured wet and dry weight over 10 days (Fig. 3D). We observed a significant decrease in normalized wet weight between day 0 and day 10 for alginate (41 ± 10 to 9 ± 5, p=0.0002) and FA IPN groups (30 ± 9 to 9 ± 3, p=0.0012), but we observed similar weights in fibrin controls between timepoints (18 ± 19 and 22 ± 14, p=0.66). On day 0, alginate possessed a greater normalized wet weight (41 ± 10) compared to fibrin control (19 ± 3) but reached similar values by day 10. IPNs exhibited similar trends on day 0 and day 10 compared to alginate controls.

Mesh size and mechanical properties are tunable *via* calcium chloride crosslinking

We characterized overall construct properties after alginate crosslinking (Fig. 4A–B). To demonstrate that IPN constructs can be molded into desired morphologies, we formed gels as previously described but in square molds. Distinct shapes cannot be discerned in fibrin gels that lose their form upon handling and transfer (Fig. 4B). Rheological measurements (Fig. 4C) revealed similar storage moduli between alginate and FA IPNs crosslinked with 10 mM $CaCl_2$ (628 ± 101 and 831 ± 205 Pa) compared to fibrin controls (250 ± 74 Pa). Alginate and FA IPNs crosslinked with 40 mM $CaCl_2$ possessed significantly increased storage moduli (3144 ± 686 and 2588 ± 1266 Pa, p=0.0001) compared to alginate and FA IPNs crosslinked with 10 mM $CaCl_2$ and fibrin controls. Average mesh size was inversely correlated with storage modulus (Fig. 4D). Mesh size decreased in alginate gels when

crosslinked with 10 mM $CaCl_2$ versus 40 mM $CaCl_2$ in alginate (23.3 ± 1.2 nm vs. 13.7 ± 1.0 nm, p=0.0002). FA IPNs exhibited a similar trend, with decreased mesh size as $CaCl_2$ concentration increased (21.3 ± 1.7 nm and 15.1 ± 2.3 nm, p=0.0027). Mesh sizes of IPNs or alginate gels were smaller than fibrin gel controls (32.2 ± 3.8 nm; $p \leq 0.0001$).

EC-MSC spreading is a function of alginate crosslinking density

We aimed to understand the contribution of fibrin and alginate crosslinking on EC and MSC spreading within IPNs using fibrinogen and EC-MSC concentrations previously established to promote *in vitro* tubule formation [18, 19]. On day 3 of co-culture, EC and MSC spreading was a function of $CaCl_2$ concentration, with greater spreading observed in IPNs formed with 10 mM $CaCl_2$ compared to 40 mM $CaCl_2$ (Fig. 5A). Cells in alginate controls lacking adhesion motifs exhibited spherical morphology regardless of $CaCl_2$ content, while fibrin controls supported cell spreading as expected. Quantification of total area and circularity of cells on day 3 of co-culture (Fig. 5B) support these qualitative observations and is further supported by separately studying EC and MSC populations (Suppl. Fig 1A). Quantification of total area revealed greater cell area in fibrin ($1.4\times10^5 \pm 4.1\times10^4$ μm^2) compared to alginate crosslinked with 10 mM $CaCl_2$ ($5.5\times10^4 \pm 3.4\times10^4$ μm^2; p=0.02). FA IPNs crosslinked with 10 mM $CaCl_2$ exhibited similar total cell area ($1.7\times10^5 \pm 7.9\times10^4$ μm^2) compared to fibrin, yet cell area in IPNs crosslinked with 40 mM $CaCl_2$ was significantly reduced ($4.0\times10^4 \pm 1.5\times10^4$ μm^2; p=0.001). Cell areas within alginate gels crosslinked with either 10 mM $CaCl_2$ ($5.5\times10^4 \pm 3.4\times10^4$ μm^2) or 40 mM $CaCl_2$ ($7.4\times10^4 \pm 1.5\times10^4$ μm^2) were comparable. Circularity revealed overall cell shape of cell populations within these gels, with circularity of 1.0 representing cells with symmetrical circular properties. Cells in fibrin controls (0.46 ± 0.02) had lower circularity versus alginate controls crosslinked with 10 mM $CaCl_2$ (0.79 ± 0.11; p=0.0001) and 40 mM $CaCl_2$ (0.82 ± 0.04; p=0.0001), confirming the ability of fibrin gels to support cell adhesion and spreading. FA IPNs crosslinked with 10 mM $CaCl_2$ (0.56 ± 0.03) resulted in intermediate circularity values between fibrin and alginate controls, while IPNs crosslinked with 40 mM $CaCl_2$ (0.77 ± 0.09) induced similar circularity values to both alginate controls. To understand whether fibrin networks within these constructs may be instructing these differences, we observed fibrin structure on day 3 of co-culture with light reflection microscopy (Fig. 5C). As expected, we did not observe fiber structures within alginate controls with light reflection, while dense, mesh structures were observed throughout fibrin gels encapsulating both cell types. In IPN hydrogels, we observed similar fibers, although less dense compared to fibrin controls. Furthermore, fibrin fibers were more apparent in IPNs crosslinked with 40 mM $CaCl_2$ compared to those with 10 mM $CaCl_2$.

EC network retention is a function on fibrinogen content within FA IPNs

Since alginate crosslinking density affects the degree of EC and MSC spreading, we investigated the role of fibrin on network formation when keeping crosslinking density constant. We formed IPNs with 10 mM $CaCl_2$ while varying the amount of fibrinogen incorporated in the FA IPN (5, 10, and 20 mg/mL). We quantified cell area and morphology collectively (Fig. 6B–C) and separately by population (Suppl. Fig 1B). EC network formation on day 3 was inversely correlated with fibrinogen concentration in fibrin gels (Fig. 6A). We observed increases in cell area in fibrin controls compared to alginate controls and

IPNs crosslinked with 40 mM $CaCl_2$ (Fig. 6B). Cell area was similar in FA IPNs crosslinked with 10 mM $CaCl_2$ compared to fibrin controls, regardless of fibrinogen content. Measurement of cell circularity revealed a similar trend (Fig. 6C), with no dependence of circularity on fibrinogen concentration in fibrin gels or FA IPNs. However, network formation was maintained in groups with increased fibrinogen on day 7, supported by phalloidin staining to detect F-actin, which signifies stress fiber formation (Fig. 6D). FA IPNs with 5 mg/mL fibrinogen exhibited little F-actin expression. Cells entrapped in FA IPNs with 10 and 20 mg/mL fibrinogen exhibited increased F-actin expression with increased spreading and distinct, stretched morphology of stress fibers. We continued characterization with FA IPNs made with 20 mg/mL fibrinogen in experiments going forward.

EC-MSC viability and function is maintained through long term culture in FA IPNs

We performed qPCR to examine gene expression of vascular endothelial growth factor (*VEGFA*), which encodes for VEGF, after 7 days of culture to investigate how angiogenic growth factor expression is influenced by FA IPNs (Fig. 7A). We observed striking differences in *VEGFA* across groups, with higher expression for cells within alginate versus fibrin gels (0.36 ± 0.08 and 0.08 ± 0.02, p=0.0004). *VEGFA* expression increased as a function of $CaCl_2$ concentration in FA IPNs.

We examined EC- and MSC-specific markers on Day 0 and 14 (Fig. 7B) to monitor changes in cellular organization over time. We observed increased network formation by CD31 staining in FA IPNs crosslinked with 10 mM $CaCl_2$ compared to alginate and IPNs crosslinked with 40 mM $CaCl_2$. αSMA expression was clear in fibrin control gels and FA IPN constructs crosslinked with 10 mM $CaCl_2$. Minimal αSMA was observed in alginate and FA IPNs crosslinked with 40 mM $CaCl_2$.

We examined changes in metabolic activity, storage modulus, and cell viability over 14 days. On Day 0, we observed greater metabolic activity in co-cultured cells entrapped in FA IPNs crosslinked with 40 mM $CaCl_2$ compared to FA IPNs crosslinked with 10 mM $CaCl_2$ (24.4% ± 4.7% and 20.4% ± 1.1% reduction; p=0.03) (Suppl. Fig. 2A). However, this was stabilized at later timepoints, with cells in fibrin gels exhibiting the greatest metabolic activity on Day 7 (45.8% ± 2.8% reduction) and Day 14 (21.2 ± 1.7) compared to all other groups. Overall metabolic activity in all gels was greatest on Day 7. Quantification of storage modulus of coculture gels over time revealed decreasing mechanical properties in all groups (Suppl. Fig. 2B), with the greatest decrease over 14 days in both alginate and FA IPNs crosslinked with 40 mM $CaCl_2$. LIVE/DEAD staining confirmed the maintenance of viable cells in FA IPNs through Day 14 (Suppl. Fig. 2C). Although more dead cells were evident within fibrin gels at Day 7, few dead cells were visible at Day 14. Cell viability in FA IPNs crosslinked with 10 mM $CaCl_2$ was comparable to fibrin controls on Day 14.

DISCUSSION

Hydrogels have tunable characteristics for adhesion, mechanical properties, and degradation, making them valuable platforms to mimic the native extracellular matrix (ECM). Standard hydrogel formulations are often formed of a single polymer, limiting their tunability as a

function of composition. However, hydrogels utilizing matricellular proteins such as collagen rely on the concentration of the polymer to drive mechanical and structural properties, while substrates using fibrin require one-step protocols for rapid crosslinking and gelation. IPN hydrogels enable a preferred embodiment of biomaterial by decoupling function from composition [23]. In this work, we formulated and characterized a fibrin-alginate IPN to independently tune adhesivity and hydrogel physical properties, which was validated by testing its capacity to support network formation by an entrapped co-culture of MSCs and ECs.

IPNs have been formed from a number of materials including collagen-alginate [10], fibrin-alginate [12], fibrin-hyaluronic acid [24], and others in order to address shortcomings of individual components. For example, collagen-alginate IPNs have been investigated for tuning stromal cell morphology and trophic factor secretion. However, collagen content and structure are limited by protein concentration [25]. Fibrin has also been employed in IPNs, as various protein and crosslinking parameters can be adjusted for desired gelation strategies [26]. Fibrin-alginate IPNs were previously used as a niche for follicle development [12], in which fibrin structure was tailored to control trophic factor secretion. Fibrin provides natural binding motifs to allow adhesion and remodeling and has been extensively used in wound healing models [27], making it an ideal component for incorporation in this IPN. While fibrin-alginate IPNs have been previously reported [12], our work extends this platform by outlining a method for full fibrin network formation before alginate crosslinking. This method decouples the gelation rates of polymers used to form the IPN, providing the opportunity to formulate IPNs using other polymers with distinctly different gelation rates. Furthermore, our FA IPNs utilize significantly lower thrombin concentrations compared to commercial fibrin glues, 2.5 U/mL compared to as high as 500 U/mL [12], to yield adequate material properties and cell response.

During the native wound healing process, thrombin cleaves fibrinogen, resulting in a dense, polymerized fibrin network. We created a fibrin network within alginate that displays such thick, uniform fibers [22]. Thrombin concentration affects fiber thickness and density within fibrin gels [28, 29], with higher concentrations resulting in thinner, yet more dense fibers [30]. Optical density within fibrin groups drastically increased at thrombin concentrations greater than 0.25 U/mL, suggesting certain thrombin thresholds are needed to initiate rapid fibrin formation. Within IPN hydrogels, we also observed distinct patterns of fibrin structure as a function of thrombin concentration. Fibrin structures in IPNs appeared thicker yet less compact compared to fibrin controls, most notably with 2.5 U/mL thrombin. We speculate that diffusion of thrombin is slower in the precursor fibrinogen-alginate solution compared to PBS due to increased viscosity. This is supported by our data on gelation kinetics, as IPNs exhibit reduced O.D. compared to respective fibrin controls. In all groups, we observed saturation in fibrin crosslinking through plateaus in gelation kinetics, suggesting that although thrombin dynamics act at different rates, we allowed sufficient time for complete thrombin activity. These findings establish that manipulation of thrombin concentration is a novel method to influence fibrin arrangement within fibrin-alginate IPNs.

Although the availability of binding sites for cells is critical for cell attachment and function, the bulk properties of hydrogels play an equally important role. Alginate is widely used as a

platform to study the effect of mechanical cues because the gelation [31, 32], swelling ratio [33], crosslinking density, and resultant moduli [34] can be easily tuned by calcium ion concentration. Thus, the degree of alginate crosslinking is another critical component for tuning cell response within this IPN. We observed increases in hydrogel storage modulus, corresponding with decreases in mesh density, as the concentration of $CaCl_2$ increased. Furthermore, alginate crosslinking density affected MSC and EC spreading. We observed greater cell spreading and tubule formation within IPNs crosslinked with lower $CaCl_2$ concentrations. Compared to fibrin gels, we observed rapid degradation of IPNs and alginate controls, suggesting alginate is degrading in our system. This was observed in both acellular and coculture experiments. We and others have emphasized the importance of construct degradation and proteolytic cleavage kinetics suitable for cell spreading and differentiation [28, 35, 36]. The differences in IPN hydrogel bulk properties crosslinked with 10 mM or 40 mM $CaCl_2$ were driven by multiple variables including degradation and mesh size. These two parameters work in concert to present adhesion sites, enable solute diffusion through the polymer network, and ultimately, create a dynamic environment. Substrate biophysical properties can also influence the production of trophic factors by entrapped cells, supported by increases in *VEGFA* expression as a function of crosslinking density in these gels. Previous work has established the importance of bulk properties of hydrogels on VEGF production and signaling for angiogenesis in wound healing [37, 38] and tumor vasculature applications [39, 40], further supporting our work in tuning mechanical properties for manipulating cell response. While these data stress the importance of mesh structure and alginate degradation on EC and stromal response in these polymer networks, it also reveals that alginate stiffness is a limiting factor of FA IPN integrity. Thus, other methods to influence stiffness once cell networks are formed may be necessary.

In order to develop a functional IPN, we established a novel method for adding fibrinogen to the polymer formulation, enabling a method to tailor the adhesivity and bulk mechanical properties of a clinically relevant hydrogel. While we interrogated elements of mesh size to understand the role of structure on cell response, the applied analytical formula is limited in its complexity. The mesh structure between alginate and fibrin are significantly different, with alginate exhibiting mesh sizes on the nanometer scale and fibrin on the micrometer scale. Thus, the nanometer range of our reported mesh size is most likely dictated by the alginate-dominant regions of the FA IPNs. Full investigation *via* advanced microscopy could be used to reveal the true structure morphology of alginate and fibrin in its hydrated form. Although simplified, our reports on mesh size highlight the interplay between structural and mechanical properties on tailoring cell response. Furthermore, outputs for cell response (*e.g.*, area and circularity) are 2D in nature, not fully describing its 3D network capacity. Nonetheless, we believe clear conclusions can be drawn through these parameters to characterize how cells interact with the IPNs.

This fibrin-alginate IPN formulation is an elegant method to modulate cell adhesion through controlling ligand availability and fibrillar structure within another polymer that regulates bulk mechanical properties. These results provide new insight into the role of fibrin presentation and crosslinking density in alginate and address critical issues for hydrogel development. Moreover, these data emphasize the connection between gel stiffness and

mesh size to influence cell response. This material may find broad utility for studying cell responses in hydrogels with different stiffnesses and as a cell transplantation vehicle.

Supplementary Material

Refer to Web version on PubMed Central for supplementary material.

ACKNOWLEDGEMENTS

Research reported in this publication was supported by National Institute of Dental and Craniofacial Research of the National Institutes of Health under award numbers R01 DE025475 and R01 DE025899 (JKL). CEV was supported by the NHLBI Training Program in Basic and Translational Cardiovascular Science (T32 HL086350). TGF was supported by the American Heart Association Postdoctoral Fellowship (19POST34460034). The content is solely the responsibility of the authors and does not necessarily represent the official views of the National Institutes of Health. We are grateful to Prof. Eduardo Silva for cord blood-derived endothelial cells. The graphical abstract and Figure 1 was created with Biorender.com.

REFERENCES

[1]. Ahmed TA, Dare EV, Hincke M, Fibrin: a versatile scaffold for tissue engineering applications, Tissue Eng Part B Rev 14(2) (2008) 199–215. [PubMed: 18544016]

[2]. Vorwald CE, Murphy KC, Leach JK, Restoring vasculogenic potential of endothelial cells from diabetic patients through spheroid formation, Cell. Mol. Bioeng 11(4) (2018) 267–278. [PubMed: 30416603]

[3]. Murphy KC, Whitehead J, Zhou D, Ho SS, Leach JK, Engineering fibrin hydrogels to promote the wound healing potential of mesenchymal stem cell spheroids, Acta Biomater. 64 (2017) 176–186. [PubMed: 28987783]

[4]. Nakatsu MN, Davis J, Hughes CC, Optimized fibrin gel bead assay for the study of angiogenesis, J Vis Exp (3) (2007) 186.

[5]. Leach JK, Whitehead J, Materials-directed differentiation of mesenchymal stem cells for tissue engineering and regeneration, ACS Biomater Sci Eng 4(4) (2018) 1115–1127. [PubMed: 30035212]

[6]. Gonzalez-Fernandez T, Sikorski P, Leach JK, Bio-instructive materials for musculoskeletal regeneration, Acta Biomater. 96 (2019) 20–34. [PubMed: 31302298]

[7]. Sperling LH, Interpenetrating polymer networks: an overview, Interpenetrating Polymer Networks, American Chemical Society1994, pp. 3–38.

[8]. Dragan ES, Design and applications of interpenetrating polymer network hydrogels. A review, Chem. Eng. J 243 (2014) 572–590.

[9]. Branco da Cunha C, Klumpers DD, Li WA, Koshy ST, Weaver JC, Chaudhuri O, Granja PL, Mooney DJ, Influence of the stiffness of three-dimensional alginate/collagen-I interpenetrating networks on fibroblast biology, Biomaterials 35(32) (2014) 8927–36. [PubMed: 25047628]

[10]. Mahou R, Vlahos AE, Shulman A, Sefton MV, Interpenetrating alginate-collagen polymer network microspheres for modular tissue engineering, Acs Biomater Sci Eng 4(11) (2018) 3704–3712.

[11]. Wisdom K, Chaudhuri O, 3D cell culture in interpenetrating networks of alginate and rBM matrix, Methods Mol. Biol 1612 (2017) 29–37. [PubMed: 28634933]

[12]. Shikanov A, Xu M, Woodruff TK, Shea LD, Interpenetrating fibrin-alginate matrices for in vitro ovarian follicle development, Biomaterials 30(29) (2009) 5476–5485. [PubMed: 19616843]

[13]. Ghajar CM, Blevins KS, Hughes CC, George SC, Putnam AJ, Mesenchymal stem cells enhance angiogenesis in mechanically viable prevascularized tissues via early matrix metalloproteinase upregulation, Tissue Eng 12(10) (2006) 2875–88. [PubMed: 17518656]

[14]. Boontheekul T, Kong HJ, Mooney DJ, Controlling alginate gel degradation utilizing partial oxidation and bimodal molecular weight distribution, Biomaterials 26(15) (2005) 2455–65. [PubMed: 15585248]

[15]. Carr ME, Hermans J, Size and density of fibrin fibers from turbidity, Macromolecules 11(1) (1978) 46–50. [PubMed: 621951]

[16]. Li J, Mooney DJ, Designing hydrogels for controlled drug delivery, Nat Rev Mater 1(12) (2016).

[17]. Williams PA, Stilhano RS, To VP, Tran L, Wong K, Silva EA, Hypoxia augments outgrowth endothelial cell (OEC) sprouting and directed migration in response to sphingosine-1-phosphate (S1P), PLoS One 10(4) (2015).

[18]. Vorwald CE, Joshee S, Leach JK, Spatial localization of endothelial cells in heterotypic spheroids influences Notch signaling, J. Mol. Med. (Berl.) (2020).

[19]. Chen XF, Aledia AS, Popson SA, Him L, Hughes CCW, George SC, Rapid anastomosis of endothelial progenitor cell-derived vessels with host vasculature is promoted by a high density of cotransplanted fibroblasts, Tissue Eng Pt A 16(2) (2010) 585–594.

[20]. van de Pol V, Bons LR, Lodder K, Kurakula KB, Sanchez-Duffhues G, Siebelink H-MJ, Roos-Hesselink JW, DeRuiter MC, Goumans M-J, Endothelial colony forming cells as an autologous model to study endothelial dysfunction in patients with a bicuspid aortic valve, Int. J. Mol. Sci 20(13) (2019) 3251.

[21]. Carrion B, Janson IA, Kong YP, Putnam AJ, A safe and efficient method to retrieve mesenchymal stem cells from three-dimensional fibrin gels, Tissue Eng Part C-Me 20(3) (2014) 252–263.

[22]. Li W, Sigley J, Pieters M, Helms CC, Nagaswami C, Weisel JW, Guthold M, Fibrin fiber stiffness is strongly affected by fiber diameter, but not by fibrinogen glycation, Biophys. J 110(6) (2016) 1400–1410. [PubMed: 27028649]

[23]. Li JY, Illeperuma WBK, Suo ZG, Vlassak JJ, Hybrid hydrogels with extremely high stiffness and toughness, ACS Macro Lett. 3(6) (2014) 520–523.

[24]. Lee F, Kurisawa M, Formation and stability of interpenetrating polymer network hydrogels consisting of fibrin and hyaluronic acid for tissue engineering, Acta Biomater. 9(2) (2013) 5143–5152. [PubMed: 22943886]

[25]. Suri S, Schmidt CE, Cell-laden hydrogel constructs of hyaluronic acid, collagen, and laminin for neural tissue engineering, Tissue Eng Part A 16(5) (2010) 1703–16. [PubMed: 20136524]

[26]. Weber M, Gonzalez de Torre I, Moreira R, Frese J, Oedekoven C, Alonso M, Rodriguez Cabello CJ, Jockenhoevel S, Mela P, Multiple-step injection molding for fibrin-based tissue-engineered heart valves, Tissue Eng Part C-Me 21(8) (2015) 832–40.

[27]. Mosesson MW, Siebenlist KR, Meh DA, The structure and biological features of fibrinogen and fibrin, Ann. N. Y. Acad. Sci 936 (2001) 11–30. [PubMed: 11460466]

[28]. Davis HE, Miller SL, Case EM, Leach JK, Supplementation of fibrin gels with sodium chloride enhances physical properties and ensuing osteogenic response, Acta Biomater. 7(2) (2011) 691–699. [PubMed: 20837168]

[29]. Leach JK, Patterson E, O'Rear EA, Distributed intraclot thrombolysis: mechanism of accelerated thrombolysis with encapsulated plasminogen activators, J. Thromb. Haemost 2(9) (2004) 1548–1555. [PubMed: 15333029]

[30]. Ryan EA, Mockros LF, Weisel JW, Lorand L, Structural origins of fibrin clot rheology, Biophys. J 77(5) (1999) 2813–26. [PubMed: 10545379]

[31]. Hati AG, Bassett DC, Ribe JM, Sikorski P, Weitz DA, Stokke BT, Versatile, cell and chip friendly method to gel alginate in microfluidic devices, Lab Chip 16(19) (2016) 3718–3727. [PubMed: 27546333]

[32]. Bassett DC, Hati AG, Melo TB, Stokke BT, Sikorski P, Competitive ligand exchange of crosslinking ions for ionotropic hydrogel formation, J Mater Chem B 4(37) (2016) 6175–6182. [PubMed: 32263629]

[33]. Matyash M, Despang F, Ikonomidou C, Gelinsky M, Swelling and mechanical properties of alginate hydrogels with respect to promotion of neural growth, Tissue Eng Part C-Me 20(5) (2014) 401–411.

[34]. Lee KY, Mooney DJ, Alginate: properties and biomedical applications, Prog Polym Sci 37(1) (2012) 106–126. [PubMed: 22125349]

[35]. Madl CM, Katz LM, Heilshorn SC, Tuning bulk hydrogel degradation by simultaneous control of proteolytic cleavage kinetics and hydrogel network architecture, ACS Macro Lett. 7(11) (2018) 1302–1307.

[36]. Ho SS, Keown AT, Addison B, Leach JK, Cell migration and bone formation from mesenchymal stem cell spheroids in alginate hydrogels are regulated by adhesive ligand density, Biomacromolecules 18(12) (2017) 4331–4340. [PubMed: 29131587]

[37]. Wu Y, Al-Ameen MA, Ghosh G, Integrated Effects of Matrix Mechanics and Vascular Endothelial Growth Factor (VEGF) on Capillary Sprouting, Ann. Biomed. Eng 42(5) (2014) 1024–1036. [PubMed: 24558074]

[38]. Sack KD, Teran M, Nugent MA, Extracellular Matrix Stiffness Controls VEGF Signaling and Processing in Endothelial Cells, J. Cell. Physiol 231(9) (2016) 2026–2039. [PubMed: 26773314]

[39]. LaValley DJ, Zanotelli MR, Bordeleau F, Wang WJ, Schwager SC, Reinhart-King CA, Matrix stiffness enhances VEGFR-2 internalization, signaling, and proliferation in endothelial cells, Converg Sci Phys Onc 3(4) (2017).

[40]. Bordeleau F, Mason BN, Lollis EM, Mazzola M, Zanotelli MR, Somasegar S, Califano JP, Montague C, LaValley DJ, Huynh J, Mencia-Trinchant N, Abril YLN, Hassane DC, Bonassar LJ, Butcher JT, Weiss RS, Reinhart-King CA, Matrix stiffening promotes a tumor vasculature phenotype, Proc. Natl. Acad. Sci. U. S. A 114(3) (2017) 492–497. [PubMed: 28034921]

Statement of Significance

Hydrogels are widely used as drug and cell delivery vehicles and as artificial extracellular matrices to study cellular responses. However, there are limited opportunities to simultaneously control mechanical properties and degradation while mimicking the complex native adhesion motifs and ligands known to encourage cell engagement with the hydrogel. In this study, we describe a fibrin-alginate interpenetrating network (IPN) hydrogel designed to balance the compliance and provisional qualities of fibrin with the mechanical stability and tunability of alginate to interrogate these contributions on cell response. We used clinically relevant cell sources, a co-culture of endothelial cells and mesenchymal stromal cells, to test its efficacy in supporting capillary formation *in vitro*. These data demonstrate the promise of this IPN for use in tissue engineering.

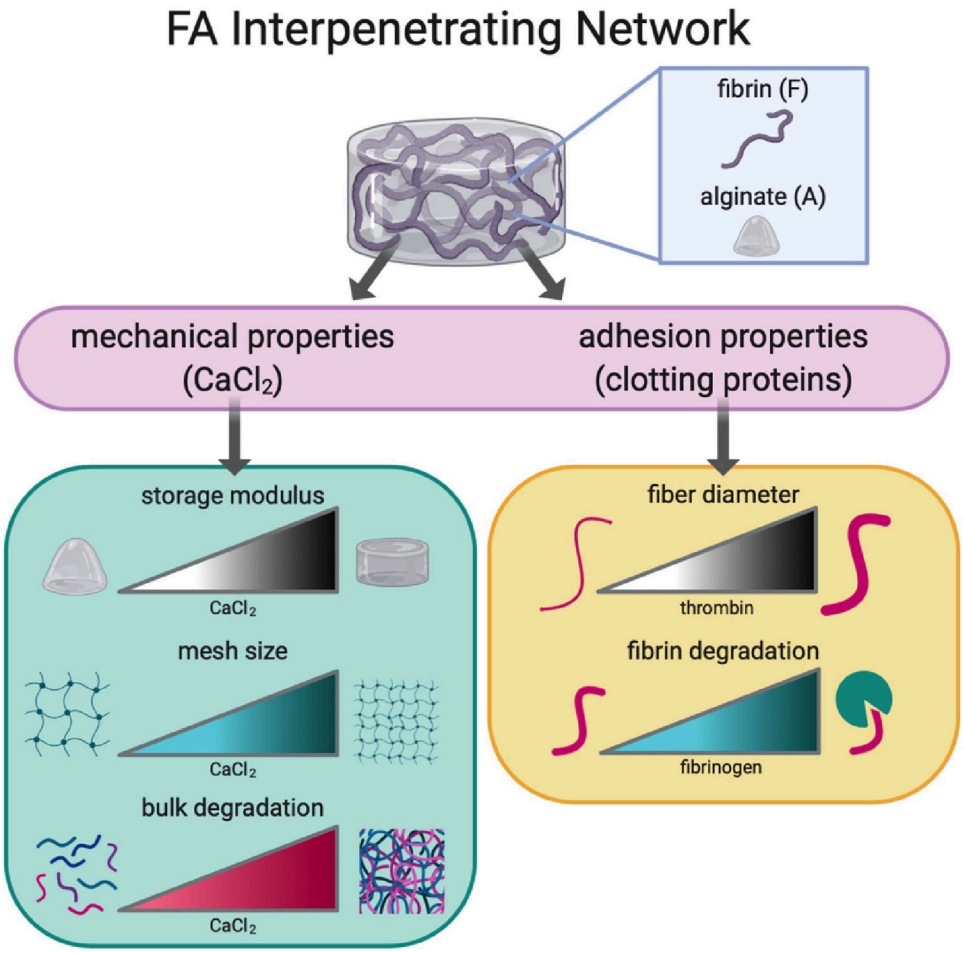

Figure 1. Schematic of parameters used to tune biophysical properties and characteristics of FA IPNs.

Tuning of mechanical and adhesion properties affects polymer structure and cell response.

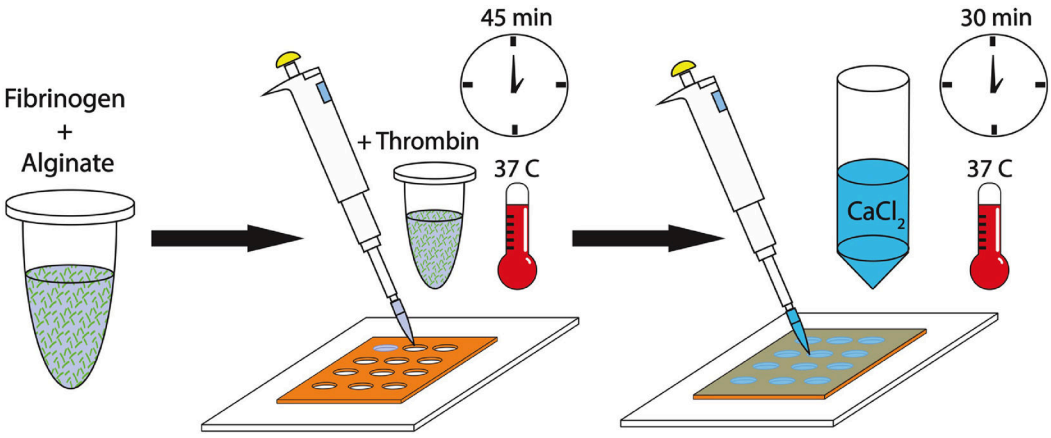

Figure 2. Experimental outline of FA IPN fabrication.

Fibrinogen and alginate are combined to generate fibrin-alginate (FA) IPNs. Independent crosslinking mechanisms are initiated through the addition of fibrin and $CaCl_2$.

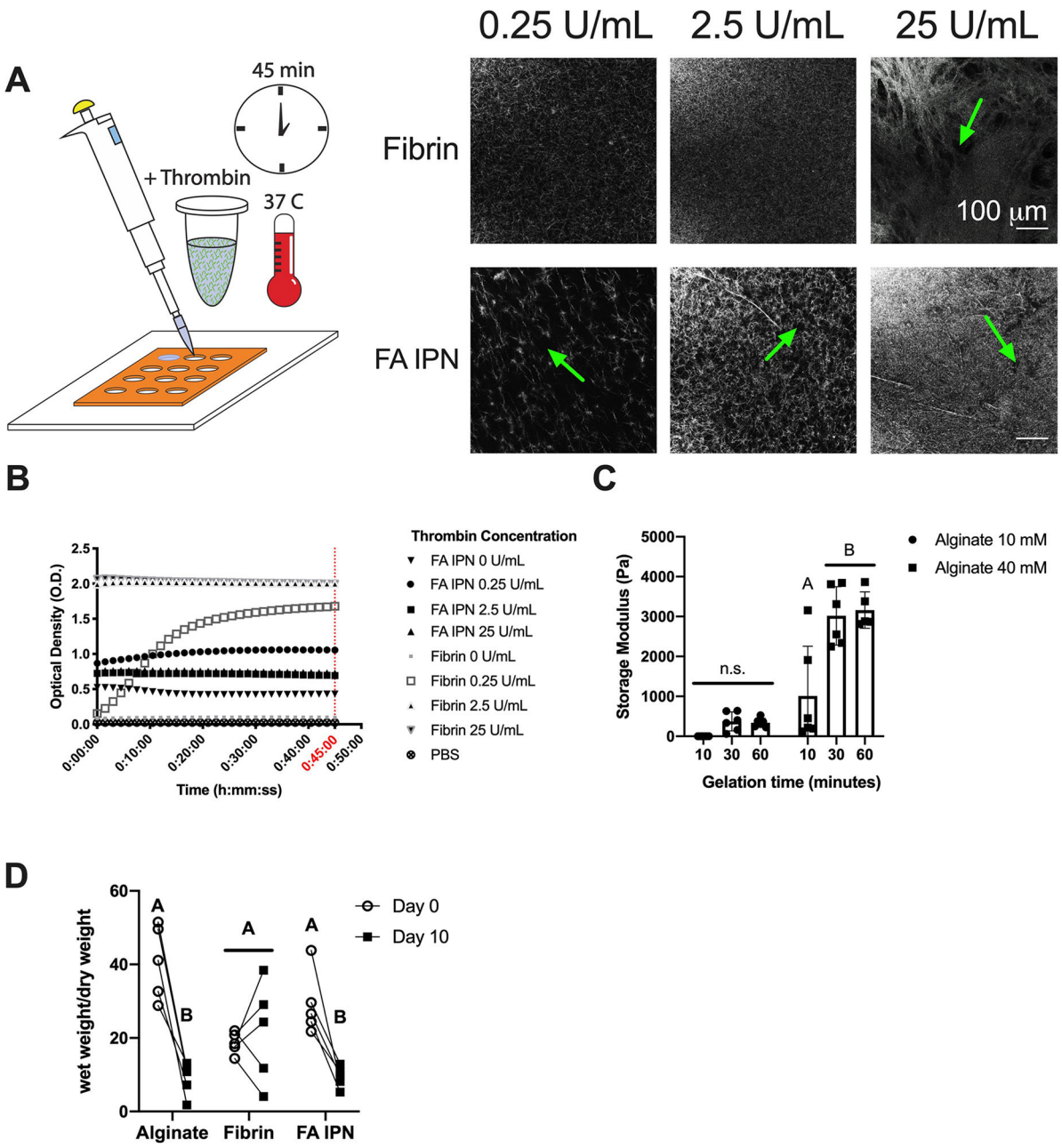

Figure 3. Fibrin structure and gelation kinetics in alginate are dependent upon thrombin concentration.

(A) Schematic and representative images of fibrin structure investigated using light reflection microscopy with varying thrombin concentrations. Green arrows indicate the presence of open pockets within the IPN. **(B)** Optical density of fibrin and FA IPNs at 550 nm (n=4–5). **(C)** Storage modulus of alginate constructs with varying $CaCl_2$ concentrations and crosslinking times. **(D)** Wet weight normalized to dry weight of constructs cultured over 10 days (n=5). Different letters denote statistical significance ($p<0.05$).

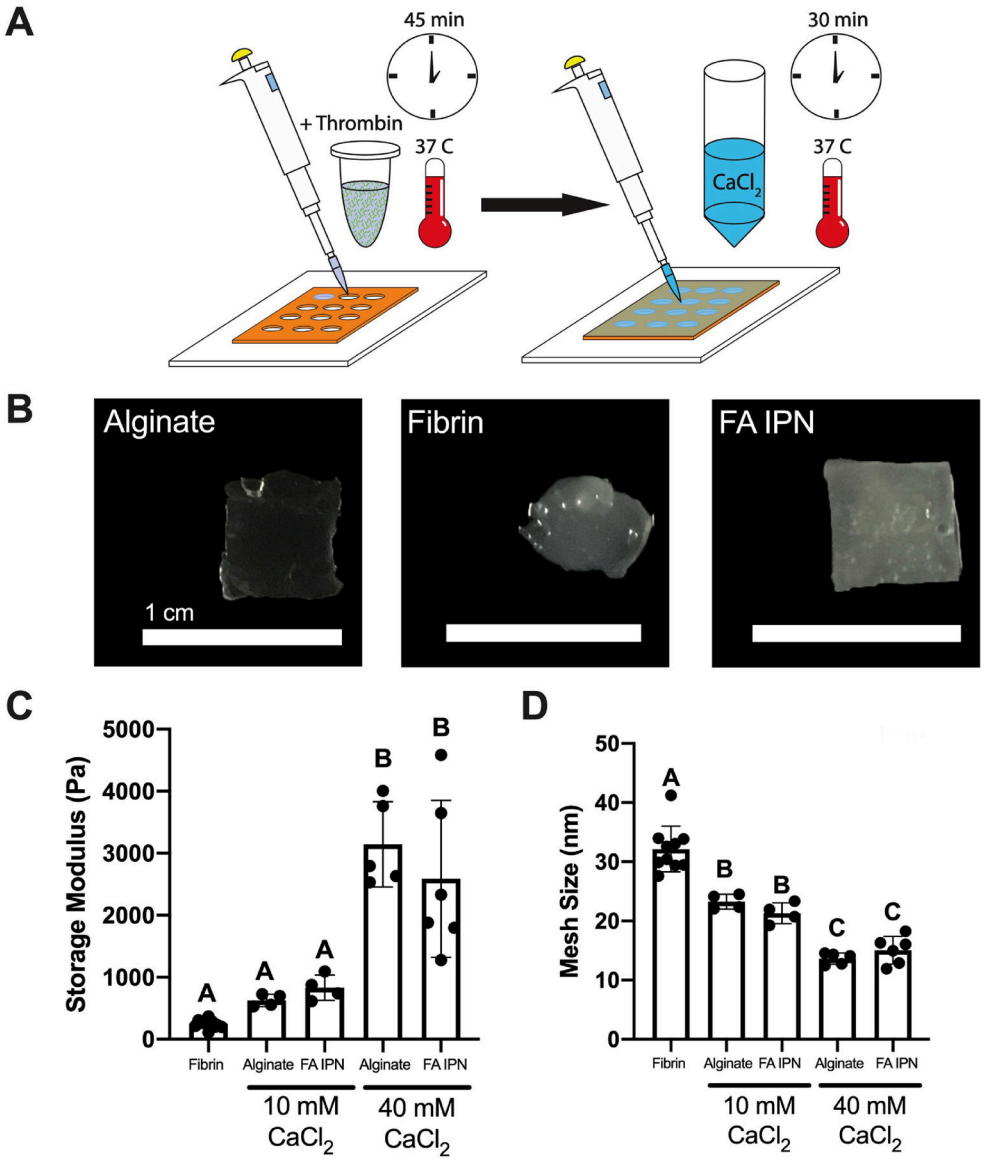

Figure 4. Material characterization of FA IPNs as a function of calcium chloride concentration.

(A) Schematic of FA IPN fabrication. (**B**) Images of resulting constructs after 30 min of gelation with 40 mM $CaCl_2$ and transfer. (**C**) Storage modulus and **(D)** calculated mesh size of FA IPNs with varying calcium chloride concentration (n=4–10). Different letters denote statistical significance ($p<0.05$).

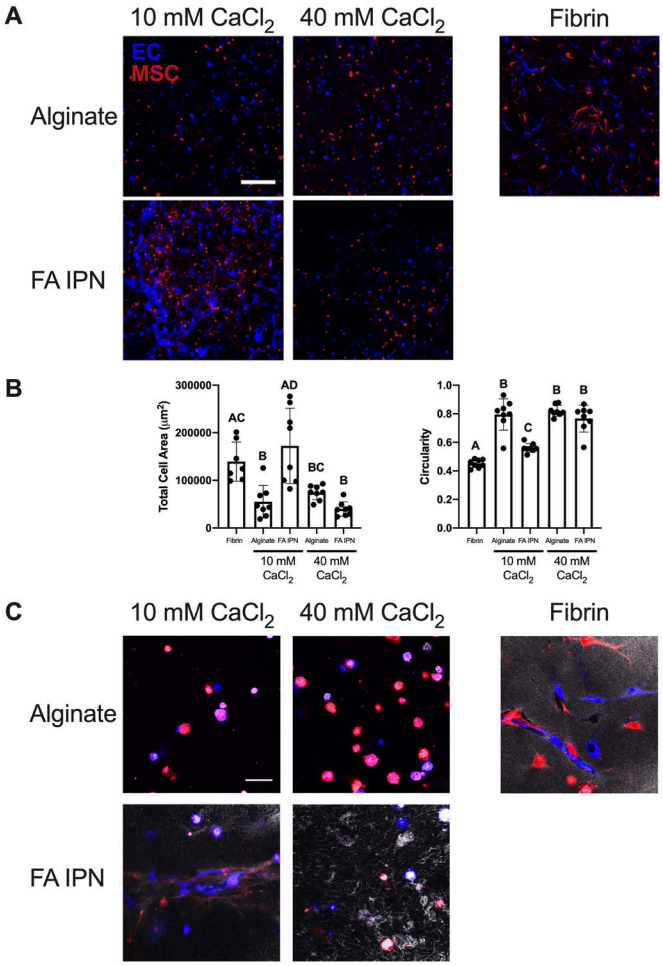

Figure 5. Alginate crosslinking density affects EC-MSC response *in vitro*.

(A) Confocal images of ECs (violet) and MSCs (red) on day 3 of culture. Scale bars are 250 μm. **(B)** Quantification of total cell area and circularity at day 3 (n=7–8). Different letters denote statistical significance ($p<0.05$). **(C)** Confocal images of fibrin structure (grayscale) with ECs (violet) and MSCs (red) at day 3. Scale bars are 50 μm.

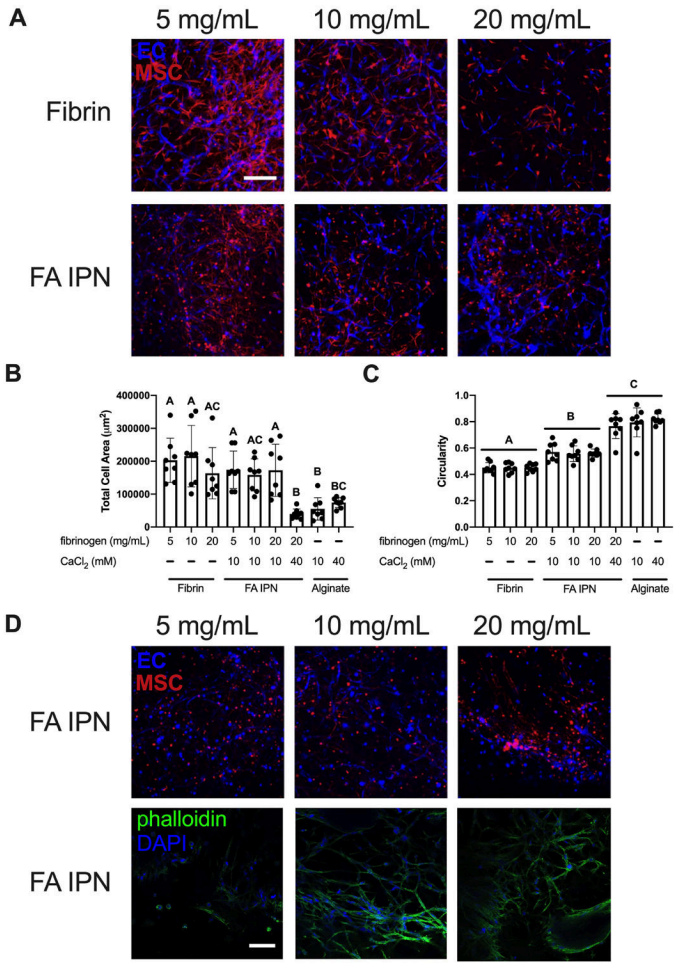

Figure 6. Fibrin content affects EC-MSC network formation and retention.

(A) Confocal images of ECs (violet) and MSCs (red) in FA IPNs with varying fibrinogen content on day 3 of culture. Scale bars are 250 μm. **(B)** Quantification of total area and **(C)** circularity (1.0 indicates a perfect circle) of ECs and MSCs in field of view on day 3 of culture (n=8). Different letters denote statistical significance (p<0.05). **(D)** Confocal images of ECs (violet) and MSCs (red) in FA IPNs (top) with respective phalloidin (green) and DAPI (violet) staining (bottom) on day 7. Scale bars are 250 μm.

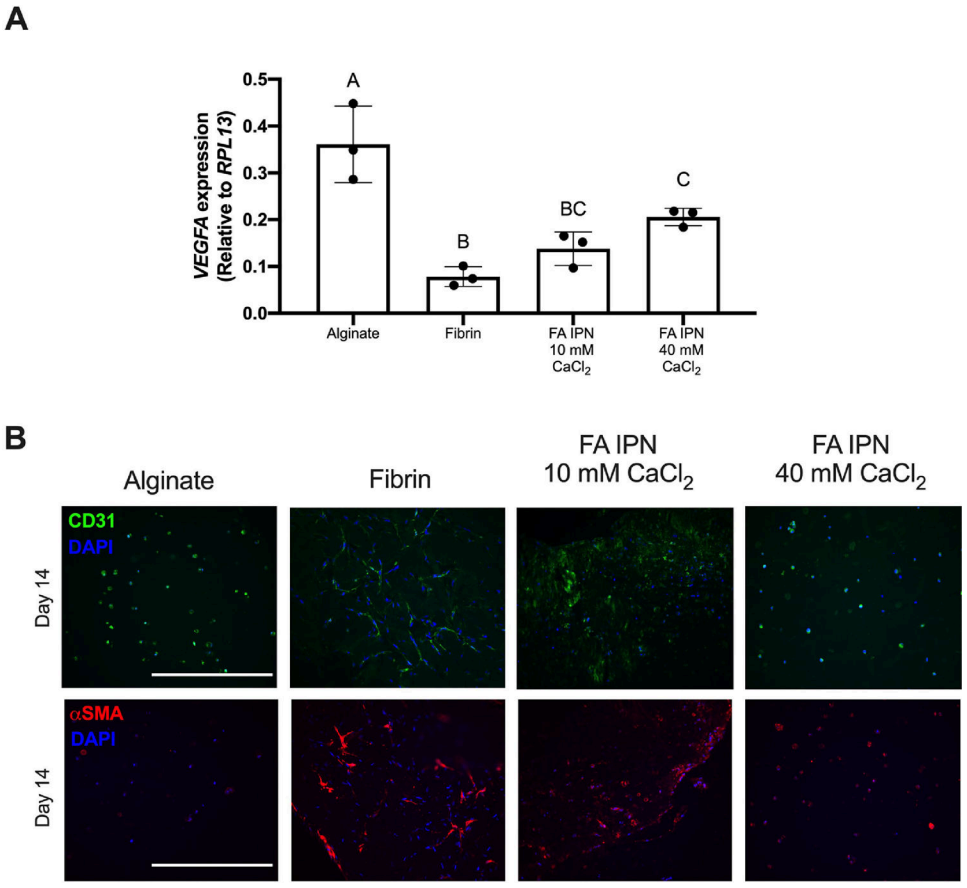

Figure 7. FA IPNs maintain EC-MSC function over time.

(A) *VEGFA* expression of EC-MSC coculture in gels on Day 7 (n=3). Different letters denote statistical significance ($p<0.05$). **(B)** CD31 (top) and SMA (bottom) staining on gels at Day 14. CD31 is green, SMA is red, and DAPI is blue. Scale bars are 200 μm.